ECS Transactions, 75 (14) 89-100 (2016)
10.1149/07514.0089ecst ©The Electrochemical Society

Accelerated Degradation of Polymer Electrolyte Membrane Fuel Cell Gas Diffusion Layers: Mass Transport Resistance and Liquid Water Accumulation at Limiting Current Density with in operando Synchrotron X-ray Radiography

Michael G. George[a], Hang Liu[a], Rupak Banerjee[a], Nan Ge[a], Pranay Shrestha[a], Dan Muirhead[a] Jongmin Lee[a],, Stéphane Chevalier[a], James Hinebaugh[a], Matthias Messerschmidt[c], Roswitha Zeis[b], Joachim Scholta[c], Aimy Bazylak[a]

[a] Thermofluids for Energy and Advanced Materials Laboratory, Dept. of Mechanical & Industrial Engineering, University of Toronto, Toronto, Ontario, M5S 3G8, Canada
[b] Karlsruhe Institute of Technology, Helmholtz Institute Ulm, Ulm, Germany
[c] Zentrum für Sonnenenergie- und Wasserstoff-Forschung Baden-Württemberg, Ulm Germany

An SGL 29BC gas diffusion layer (GDL) was degraded (aged) in hydrogen peroxide. The impact of ageing was measured through deviations from pristine GDLs in terms of limiting current densities, oxygen mass transport resistances, and liquid water spatial distributions in the GDL. For dry and saturated cathode conditions (oxygen concentrations of 1% and 21%, respectively) the fuel cell containing the aged GDL reached limiting current densities that were up to 10.3% lower and experienced increases in oxygen mass transport resistance of up to 11.7% versus the pristine GDL. This performance reduction was attributed to a higher liquid water content (13% more at an oxygen concentration of 21%) in the aged GDL under the channel compared to the pristine GDL. In fuel cells built with aged and pristine GDLs, up to 200% more water was present in the GDL under the land compared to under the channel at limiting current operation.

Introduction

As polymer electrolyte membrane (PEM) fuel cell technologies approach commercial applications, particularly in the automotive industry, understanding the potential impact of fuel cell material degradation on operating efficiency and performance over time becomes increasingly important (1-4). The United States Department of Energy has set a fuel cell stack durability target of 5000 hours of operation with less than 10% voltage degradation, which has still not been met under realistic transient conditions (5). A number of studies have identified reductions in cell potential after prolonged fuel cell operation (6-9). Degradation mechanisms for PEM fuel cells include; thermal, chemical, and mechanical degradation of the membrane, sintering and dissolution of the catalyst, and chemical corrosion of carbon and polytetrafluoroethylene (PTFE) in the gas diffusion layer (GDL) and catalyst layers (1-4). However, degradation studies based on normal fuel cell operation require significant time and resources, up to 3 years of operation in some cases (6).

The significant times and resources required for degradation studies have motivated the development of accelerated degradation protocols to simulate the effects of prolonged operation, without the corresponding time commitment (10). Most accelerated ageing protocols evaluating performance consist of *in situ* procedures, such as voltage cycling and start-up/shut-down cycling (9, 11-14), where catalyst degradation has been the focus. Freeze/thaw cycling has also been performed to evaluate the effects of mechanical degradation on cell performance (15-18).

Although degradation studies are more commonly focused on the catalyst layer, GDL degradation also contributes to fuel cell performance losses (7, 8, 18-26). One of the primary functions of the GDL is to regulate water management and provide pathways for oxygen to reach the reactant sites efficiently (27, 28). Improvements to this functionality have been made by rendering the material hydrophobic with a polytetrafluoroethylene (PTFE) treatment and adding a carbon-based microporous layer (29-32). The majority of the studies investigating GDL degradation have identified increases in mass transport resistance, and/or reductions in hydrophobicity, as the primary effect of degradation (7, 8, 21-26). This loss in hydrophobicity is most likely facilitated by carbon corrosion and PTFE loss, which has been shown to affect wettability of carbon based fuel cell components (25, 33, 34). Bosomoiu et al. (21) performed one of the longest reported in situ degradation studies focused on the GDL and observed reduced GDL hydrophobicity after 1000 hours of operation.

Based on the observations of past degradation studies, multiple protocols for accelerated degradation targeting GDLs have been developed. Mechanical degradation has been implemented through compression and freeze/thaw cycling (15, 18). Although *in situ* freeze/thaw cycling can damage the membrane and catalyst layer (35), the impact of this cycling on the isolated GDL structure was minimal. Wu et al. (24) performed *in situ* ageing by applying higher reactant gas flow rates and increasing cell operating temperature for 200 hours, and they attributed increases in GDL mass transport losses to PTFE degradation in the GDL. *Ex situ* GDL degradation methods have been useful for isolating degradation effects specific to the GDL, where reductions in hydrophobicity are typically observed (20, 22, 23). Constructing fuel cells for *in situ* performance testing using GDLs that have undergone *ex situ* degradation isolates the effects of GDL degradation on total cell performance (20). However, these methodologies still required significant experimental times (up to 2160 hours).

An accelerated degradation methodology to simulate the effects of GDL degradation is by chemical corrosion (oxidation) with hydrogen peroxide. The selection of hydrogen peroxide to degrade fuel cell materials is suitable because it is an intermediate product of the oxygen reduction reaction (36). Both the formation of hydrogen peroxide and peroxide radicals within an operating fuel cell have been detected experimentally (37-39). An early study in the use of hydrogen peroxide to simulate GDL degradation was performed by Frisk et al. (26) and was later investigated by Arlt et al. (40). These studies observed reductions in cell performance due to increased mass transport losses and increased water accumulation in the GDL. Recently, a study of GDL degradation using hydrogen peroxide (performed in less than 12 hours) was described by Liu et al. (41).

The impact of GDL degradation on wettability can be evaluated through changes in mass transport losses, which are dependent on water distributions and accumulation in the

GDL (42, 43). This is of particular interest at high current densities where liquid water accumulation has been shown to significantly increase oxygen mass transport related losses (44). The two most common approaches to quantify mass transport resistance are electrochemical impedance spectroscopy (EIS) (45, 46) and limiting current studies (43, 47-50). Whereas EIS measurements simultaneously detect the activation, ohmic, and mass transport losses, a limiting current approach can be used to isolate the oxygen mass transport directly, based on the limiting current density and fuel cell operating conditions. By controlling the concentration of oxygen delivered to the cathode, the limiting current approach leads to measurement of oxygen mass transport resistances as a function of water production rates and accumulation within the fuel cell (43, 50). Baker et al. (50) examined cases of low oxygen concentration in order to measure the mass transport resistance due to the structure of the gas diffusion layers in the assumed absence of liquid water accumulation. The oxygen mass transport resistances, for various degrees of water accumulation in the GDL, have also been uniquely identified in earlier works (43).

Owejan et al. (43) combined the limiting current approach with *in situ* visualisation to correlate mass transport resistance to liquid water behavior in the GDL. By using neutron radiography, they identified the heterogeneous accumulation of water between the rib and channel regions and an increased water pooling under the ribs. Oxygen mass transport resistance was shown to increase in direct relation to water accumulation in the GDL. This suggests that the influence of GDL degradation can be evaluated in direct relation to water accumulation using *in situ* visualisation. Synchrotron X-ray radiographic visualisation techniques have also been applied to fuel cell research (44, 51-59). For example, Antonacci et al. (44) used EIS to quantify mass transport resistance and observed increasing mass transport resistance with increasing water content.

In this paper, synchrotron X-ray radiographic imaging during limiting current operation was used to evaluate the influence of accelerated artificial GDL aging on the liquid water distribution in the GDL. The limiting current densities of both aged and pristine GDLs were compared, and the distribution of liquid water in the GDL under the channel was compared to that under the land. For both aged and pristine GDLs, two oxygen concentrations, 1% and 21%, were used to evaluate oxygen mass transport resistances for dry and saturated conditions.

Methodology

GDL Accelerated Degradation

In order to facilitate accelerated degradation of the SGL 29BC gas diffusion layer through carbon corrosion, the GDL was submerged in a 35 % solution of hydrogen peroxide at 90°C for 12 hours. Following degradation, the material was rinsed and soaked for 24 hours in deionized (DI) water before being dried in a vacuum oven at 80°C. The reader is referred to the study performed by Liu et al. (41) for a thorough description of this ageing methodology.

Fuel Cell Testing Setup

In order to compare the performance of aged and pristine samples of SGL 29BC GDL, each material was assembled into an experimental fuel cell. The fuel cell used in this study was designed for through-plane synchrotron X-ray radiographic imaging and has an active

area of 0.68 cm^2 (8 mm in the beam direction and 8.5 mm perpendicular to the beam direction). It features eight parallel 0.5 mm x 0.5 mm channels separated by 0.5 mm-wide ribs. Both fuel cells were built with a commercial membrane electrode assembly that consisted of a Nafion HP membrane (Dupont, Ionpower) with a platinum loading of 0.3 mg/cm^2 in both the anode and cathode catalyst layers. In both fuel cell builds, the same GDL was used for the anode and cathode diffusion layers. For SGL 29BC, with a nominal thickness of 235 µm, a 188 µm-thick incompressible polyethylene naphthalate (PEN) gasket was used to control GDL compression. Assuming a catalyst layer thickness of 15 µm, this resulted in a reduction in thickness by 26%. Table I summarizes the operating conditions used for this study. Nitrogen gas was used to dilute the cathode gas stream (air) to achieve oxygen gas concentrations as low as 1%. Anode humidification was set to 100% relative humidity to ensure membrane hydration. All testing was performed using an 850e Fuel Cell Test System (Scribner and Associates Inc.).

Table I: Experimental settings for limiting current tests with varying oxygen concentration.

Parameter	Cell Temp. [ºC]	Gas Relative Humidity [%]	Absolute Pressure [kPa]	Gas Flow Rate SLPM	Reactant Gas	Diluting Gas	Reactant Gas Conc. [%]	Diluting Gas Conc. [%]
Anode	60	100	200	1	H_2	N/A	100	0
Cathode		80	200	1	Air	Nitrogen	100 & 5	0 & 95

Fuel Cell Testing Protocol

A limiting current approach was used to quantify the effect of accelerated degradation, specifically in terms of mass transport losses. Uniform gas concentrations were applied in the channels of the cell, and a small active area (0.68 cm^2) and high reactant stoichiometry were used. A small active area was used to ensure negligible pressure drops along the gas channels across the active area. With these design considerations, oxygen mass transport resistance was determined as follows (48-50):

$$R_T = \frac{\Delta c}{N_O} = 4F\frac{\Delta c}{i}, \quad [1]$$

where $F\ [\frac{C}{mol_e}]$ is the Faraday constant, $\Delta c\ [\frac{mol_{O2}}{cm^3}]$ is the oxygen concentration gradient between the channel and reaction sites, and $i\ [\frac{A}{cm^2}]$ is the cell current density. When the cell is operated at the limiting current, it can be assumed that the oxygen concentration at the reaction sites is effectively zero; therefore, the oxygen concentration gradient, Δc, is equal to the oxygen concentration in the cathode gas channels. Correcting for the effect of relative humidity and the partial pressure of water vapour in the cathode gas stream, the expression for oxygen mass transport resistance becomes (50);

$$R_T = \frac{4Fx_O^{dry-in}}{i_{lim}}\frac{p - p_w}{RT}, \quad [2]$$

where x_O^{dry-in} $[\frac{mol_{O2}}{mol_{gas}}]$ is the inlet dry mole fraction of oxygen, p $[Pa]$ is the total gas pressure, p_w $[Pa]$ is the partial pressure of water vapour, R $[\frac{cm^3 \cdot Pa}{mol_{gas} \cdot K}]$ is the universal gas constant, and T $[K]$ is the gas temperature. Inlet gas lines were heated, and we assumed that the gas temperature was equivalent to our cell operating temperature. For the calculation of oxygen mass transport resistance, the partial pressure of water vapor was based on a relative humidity of 80% at the cathode and an operating cell temperature of 60°C.

The limiting current approach outlined above was used to quantify the oxygen mass transport resistance at dry and partially saturated conditions in the cathode (volumetric oxygen concentrations of 1% and 21%, respectively). It was assumed that for an oxygen concentration of 1%, the oxygen mass transport resistance corresponded to the GDL structure, due to the absence of liquid water. The oxygen mass transport resistance measured for an oxygen concentration of 21% included the combined impact of the dry cathode electrode structure and the additional presence of liquid water.

Synchrotron X-ray Radiographic Imaging

The experiments in this study were performed at the Biomedical Imaging and Therapy (BMIT-BM) beamline (05B1-1 POE-2) at the Canadian Light Source (60). Images were captured by the imaging camera (OrcaFlash 4.0, Hamamatsu) with a 6.5 μm pixel resolution and a frame rate of 0.33 frames/s. All experiments were performed using a monochromatic 24 keV X-ray beam and with a spatial resolution of 10 μm.

The image that is captured by the charge-coupled device (CCD) camera was converted from a raw absorption image into a processed water thickness image to quantify the liquid water content, as seen in Figure 1. The liquid water content at each position of the image was determined from the following Beer-Lambert Law (61)

$$x_w(x,y) = \frac{-\ln\left(\frac{I(x,y)}{I_0(x,y)}\right)}{\mu_w} \quad [3]$$

where $x_w(x,y)$ $[cm]$ is the detected water thickness in the beam direction, $I(x,y)$ is the test image intensity, $I_0(x,y)$ is the reference image intensity, and μ_w $[\frac{1}{cm}]$ is the calibrated mass attenuation coefficient of water at the X-ray energy of 24 keV. Water detection using this technique involves image normalization with a "dry image" for which no liquid water is present in the GDL. This dry image is used as the reference image intensity, $I_0(x,y)$, in equation 3, and was determined by averaging 10 frames at the end of 5 minutes of open circuit voltage (OCV) operation. Details of this procedure and the calibration of the water attenuation coefficient are described in detail by Ge et al. (62). Water thickness values were then normalized by the length of the active area traversed by the X-ray beam (8 mm for the fuel cell used). Consequently, the normalized water thickness values are reported in units of water thickness χ_w $[cm]$ per active area thickness in the beam direction χ_{FC} $[cm]$.

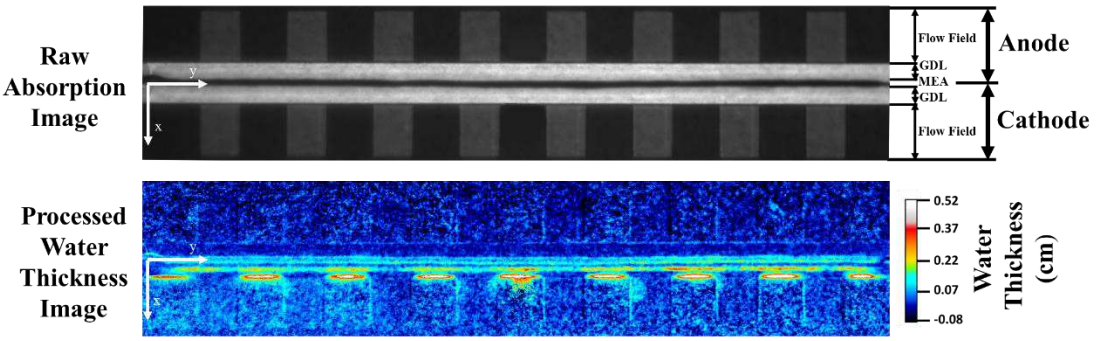

Figure 1: Representation of raw absorption image and processed water thickness image for a sample of SGL 29BC.

Results and Discussion

In this section, we first describe the effect of ageing on reducing limiting current density and increasing oxygen mass transport resistance in wet conditions. Secondly, we present synchrotron images to identify the changes in water distribution that correspond to these decreases in limiting current density and increasing oxygen mass transport resistance.

Effect of Ageing on Limiting Current Density

Figure 2 shows the polarization performance curves for both of the fuel cells built using aged and pristine GDLs in the mass transport limited region at oxygen concentrations of 1%, Figure 2a, and 21%, Figure 2b. An increased number of data points were collected at low voltages to facilitate stable fuel cell operation as the limiting current density was approached.

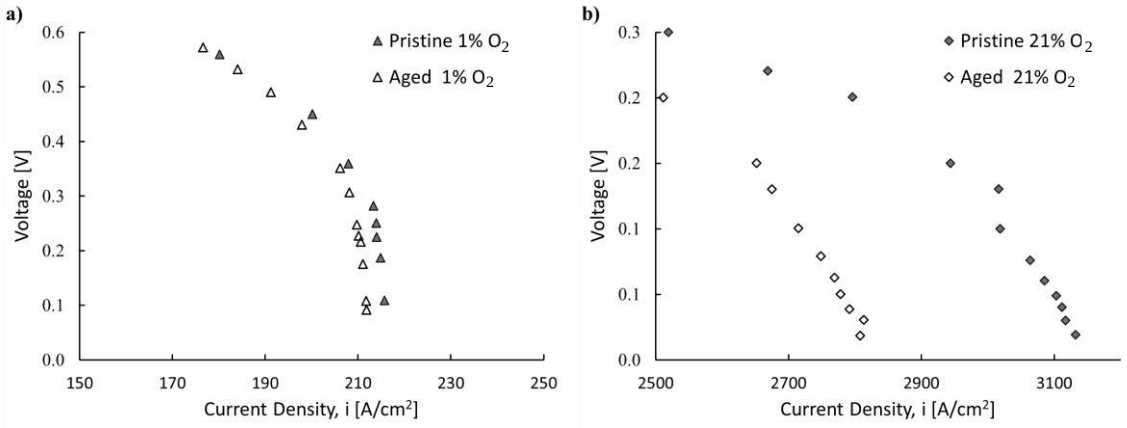

Figure 2: Polarization performance curves for aged and pristine samples of SGL 29BC for limiting current tests at anode and cathode humidification of 100% and 80% respectively, and oxygen concentrations of a) 1% and b) 21%.

Table II summarizes the limiting current densities that were achieved for both the aged and pristine fuel cell builds at both oxygen concentrations tested. In the 1% oxygen concentration cases for both aged and pristine fuel cell builds, liquid water accumulation

in the GDL was negligible and the cathode electrode was considered dry due to lower limiting current densities and water production rates. Comparing the limiting current densities in the 1% oxygen concentration cases in Table II shows that a relatively small change was observed (reduction by 1.9%), providing an indication that the GDL structure was not affected by ageing. The reduction of 10.3% in limiting current density between aged and pristine GDLs for the case with an oxygen concentration of 21% is attributed to differences in the cathode GDL water content.

Table II: Summary of experimental limiting current densities for fuel cells built using aged and pristine SGL 29BC materials.

	Limiting Current Density [mA/cm^2]		
Oxygen Concentration [volume %]	**29BC Pristine**	**29BC Aged**	**% Reduction**
1%	216	212	1.9
21%	3150	2826	10.3

Equation 2 was used to calculate the oxygen mass transport resistances at each limiting current density (Table III). As expected, for the 1% oxygen case, the mass transport resistance did not vary significantly between the aged and pristine GDLs. However, an 11.7% increase in the mass transport resistance was observed in the aged GDLs during operation with an oxygen concentration of 21%.

Table III: Oxygen mass transport resistances as a function of oxygen concentration for aged and pristine SGL 29 BC.

	Oxygen Mass Transport Resistance [s/cm]		
Oxygen Concentration [volume %]	**29BC Pristine**	**29BC Aged**	**% Increase Due to Ageing**
1%	1.25	1.27	1.6
21%	1.71	1.91	11.7
% Increase Due to Water Saturation	36.8	50.4	

Effect of Ageing on Liquid Water Distribution

In-plane synchrotron X-ray radiographic images were obtained to quantify through-plane normalized water thickness in the cathode GDL at limiting current operation. Liquid water was not observed in either GDL with an oxygen concentration of 1%. Additionally, for all cases tested, liquid water was not detected in the anode GDL.

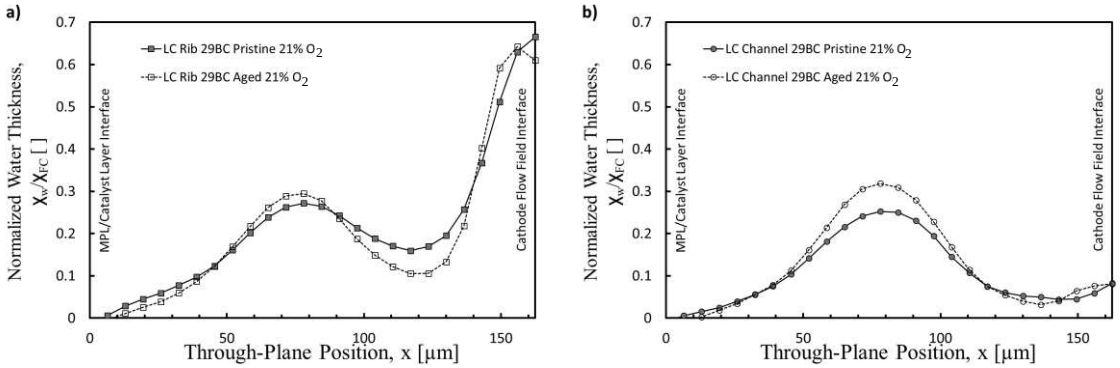

Figure 3: Normalized water profile in the cathode GDL at limiting current density for an oxygen concentration of 21% under the a) rib region and b) channel regions of the flow field.

Analysis of the normalized water distributions in the GDL was focused individually on regions of the substrate under the flow field ribs and channels with consideration of the GDL between the CL and the flow field interface. For the channel regions, although it is possible for the GDL to intrude the channel, this effect was not detected in the synchrotron images obtained. Figure 3 shows the strong degree of heterogeneity between the water profiles that are established under these rib and channel regions, which can also be observed in Figure 1. The largest difference in the accumulation of liquid water between Figure 3a and Figure 3b is observed under the rib region near the interface between the flow field and GDL (x = 162.5μm). This observation suggests that the gas transport through the GDL occurs predominantly under the channel regions, and liquid water accumulates preferentially under the rib regions.

Comparing the aged and pristine fuel cells, a significant increase in the water content of the aged GDL under the channel regions of the flow field can be identified (Figure 3b). The average normalized water thickness was calculated by averaging all pixels in the analyzed rib and channel regions (Table IV). Under the channel region of the GDL, the average normalized water thickness increased by 13.2% due to ageing. This increase in water accumulation in the aged GDL leads to increasingly restrictive gas transport due to the higher average water content and a higher maximum normalized water thickness (0.32 (aged) vs. 0.25 (pristine) located at x = 78 μm). For the rib region, average water content was reduced by 4.7% in the aged GDL, which could be related to decreased water generation rates at the catalyst layer for the reduced limiting current density. However, the local maximum normalized water thickness located at x = 78 μm in the aged GDL remained higher (0.29 (aged) vs. 0.27 (pristine)). The oxygen mass transport resistance may be dominated by the local maximum water thickness (x =78μm). Therefore, in the rib region of the GDL, even though total water content was reduced (Table IV), the increase in peak normalized water thickness in the bulk of the GDL may have had a greater effect.

Table IV: Summary of average normalized water content in the cathode GDL.

		Normalized Average Water Thickness $\frac{X_w}{X_{FC}}$ [ ]	
Sample	**Pristine 29BC**	**Aged 29BC**	**% Change with Ageing**
Oxygen Concentration	**21% O_2**	**21% O_2**	
Total Average	0.164	0.161	-1.8
Rib Region	0.215	0.205	-4.7
Channel Region	0.106	0.120	13.2

The ratios of average water thickness under the rib region to that under the channel region were 1.7 and 2.0 for the aged and pristine GDLs, respectively. A more significant reduction in channel water content, relative to the rib region, was observed for the pristine GDL. This was attributed to lower water retention in the channel region of the pristine GDL. Total average normalized water thickness (Table IV) was found to be similar between both cells at the limiting current density even though a 10.3% reduction in limiting current was observed for the aged sample at an oxygen concentration of 21%. This is likely due to a reduction in GDL hydrophobicity, imparted by chemical corrosion (oxidation) in hydrogen peroxide solution.

Conclusions

An SGL 29BC GDL was subjected to accelerated degradation in hydrogen peroxide, and its performance was compared to a pristine GDL in operando. The performance of these materials was evaluated using a coupled approach of simultaneous limiting current density and in situ synchrotron X-ray radiography measurements. Degradation resulted in a 10.3 % reduction in the limiting current of the fuel cell constructed with aged GDLs and an increase in oxygen mass transport resistance of 11.7% for an oxygen concentration of 21%. By evaluating the limiting current at an oxygen concentration of 1%, we distinguished between the structural impact of the GDL on mass transport resistance and the additional oxygen mass transport resistance associated with a partially saturated GDL. Although the total water content in the GDL was relatively unchanged for operation at an oxygen concentration of 21%, the increase in oxygen mass transport resistance for the aged GDL was attributed to the impact of ageing on the accumulation of water under the channel region of the flow field (an increase of up to 13% compared to the pristine GDL). A strong degree of heterogeneity in partially saturated GDL water distributions at limiting current was observed. These distributions are expected to influence two phase flow phenomena in the GDL and should be considered when analyzing and modelling water saturation and reactant flow in the GDL.

Acknowledgments

Graduate scholarships to Michael G. George from NSERC, the Ontario Graduate Scholarship, the Institute for Sustainable Energy, and the University of Toronto and to Hang Liu from the Connaught International Scholarship for Doctoral Students and the University of Toronto are also gratefully acknowledged. Financial support from the Natural Sciences and Engineering Research Council of Canada, the NSERC Collaborative

Research and Training Experience Program (CREATE) Program in Distributed Generation for Remote Communities, the Canada Research Chairs Program, the Ontario Ministry of Research and Innovation Early Researcher Award, and Canadian Foundation of Innovation (CFI) are gratefully acknowledged. The authors acknowledge Dr. George Belev, Dr. Adam Webb, Dr. Ning Zhu and Dr. Tomasz Wysokinski at the Canadian Light Source, in Saskatoon, SK, Canada for their generous assistance. Research described in this work was performed at the Canadian Light Source, which is supported by the Natural Sciences and Engineering Research Council of Canada (NSERC), the National Research Council Canada, the Canadian Institutes of Health Research, the Province of Saskatchewan, Western Economic Diversification Canada, and the University of Saskatchewan.

References

1. R. Borup, J. Meyers, B. Pivovar, Y. S. Kim, R. Mukundan, N. Garland, D. Myers, M. Wilson, F. Garzon and D. Wood, *Chem.Rev.*, **107**, 10 (2007).
2. F. De Bruijn, V. Dam and G. Janssen, *Fuel cells.*, **8**, 1 (2008).
3. J. Wu, X. Z. Yuan, J. J. Martin, H. Wang, J. Zhang, J. Shen, S. Wu and W. Merida, *J.Power Sources.*, **184**, 1 (2008).
4. N. Garland, T. Benjamin and J. Kopasz, *ECS Transactions.*, **11**, 1 (2007).
5. U.S. Drive, **June 2016**, 06/25 (June 2013).
6. S. Cleghorn, D. Mayfield, D. Moore, J. Moore, G. Rusch, T. Sherman, N. Sisofo and U. Beuscher, *J.Power Sources.*, **158**, 1 (2006).
7. Y. Hiramitsu, H. Sato, H. Hosomi, Y. Aoki, T. Harada, Y. Sakiyama, Y. Nakagawa, K. Kobayashi and M. Hori, *J.Power Sources.*, **195**, 2 (2010).
8. D. L. Wood and R. L. Borup, *J.Electrochem.Soc.*, **157**, 8 (2010).
9. C. Hartnig and T. J. Schmidt, *J.Power Sources.*, **196**, 13 (2011).
10. X. Yuan, H. Li, S. Zhang, J. Martin and H. Wang, *J.Power Sources.*, **196**, 22 (2011).
11. J. C. Meier, C. Galeano, I. Katsounaros, A. A. Topalov, A. Kostka, F. Schüth and K. J. Mayrhofer, *Acs Catalysis.*, **2**, 5 (2012).
12. D. Liu and S. Case, *J.Power Sources.*, **162**, 1 (2006).
13. S. Lee, E. Cho, J. Lee, H. Kim, T. Lim, I. Oh and J. Won, *J.Electrochem.Soc.*, **154**, 2 (2007).
14. J. Kim, J. Lee and Y. Tak, *J.Power Sources.*, **192**, 2 (2009).
15. M. Luo, C. Huang, W. Liu, Z. Luo and M. Pan, *Int J Hydrogen Energy.*, **35**, 7 (2010).
16. S. Kim, B. K. Ahn and M. Mench, *J.Power Sources.*, **179**, 1 (2008).
17. S. Lim, G. Park, J. Park, Y. Sohn, S. Yim, T. Yang, B. K. Hong and C. Kim, *Int J Hydrogen Energy.*, **35**, 23 (2010).
18. C. Lee and W. Mérida, *J.Power Sources.*, **164**, 1 (2007).
19. W. Schmittinger and A. Vahidi, *J.Power Sources.*, **180**, 1 (2008).
20. G. Chen, H. Zhang, H. Ma and H. Zhong, *Int J Hydrogen Energy.*, **34**, 19 (2009).
21. M. Bosomoiu, G. Tsotridis and T. Bednarek, *J.Power Sources.*, **285** (2015).
22. S. Kandlikar, M. Garofalo and Z. Lu, *Fuel Cells.*, **11**, 6 (2011).
23. J. Cho, T. Ha, J. Park, H. Kim, K. Min, E. Lee and J. Jyoung, *Int J Hydrogen Energy.*, **36**, 10 (2011).
24. J. Wu, J. J. Martin, F. P. Orfino, H. Wang, C. Legzdins, X. Yuan and C. Sun, *J.Power Sources.*, **195**, 7 (2010).

25. T. Ha, J. Cho, J. Park, K. Min, H. Kim, E. Lee and J. Jyoung, *Int J Hydrogen Energy.*, **36**, 19 (2011).
26. J. Frisk, M. Hicks, R. Atanasoski, W. Boand, A. Schmoeckel and M. Kurkowski, *MEA component durability.*, (2004).
27. L. Cindrella, A. Kannan, J. Lin, K. Saminathan, Y. Ho, C. Lin and J. Wertz, *J.Power Sources.*, **194**, 1 (2009).
28. U. Pasaogullari and C. Wang, *J.Electrochem.Soc.*, **151**, 3 (2004).
29. H. K. Atiyeh, K. Karan, B. Peppley, A. Phoenix, E. Halliop and J. Pharoah, *J.Power Sources.*, **170**, 1 (2007).
30. J. T. Gostick, M. A. Ioannidis, M. W. Fowler and M. D. Pritzker, *Electrochemistry Communications.*, **11**, 3 (2009).
31. A. Thomas, G. Maranzana, S. Didierjean, J. Dillet and O. Lottin, *Int J Hydrogen Energy.*, **39**, 6 (2014).
32. S. Shimpalee, U. Beuscher and J. Van Zee, *Electrochim.Acta.*, **52**, 24 (2007).
33. H. Chizawa, Y. Ogami, H. Naka, A. Matsunaga, N. Aoki and T. Aoki, *ECS Transactions.*, **3**, 1 (2006).
34. K. H. Kangasniemi, D. Condit and T. Jarvi, *J.Electrochem.Soc.*, **151**, 4 (2004).
35. S. Kim and M. Mench, *J.Power Sources.*, **174**, 1 (2007).
36. M. K. Debe, *Nature.*, **486**, 7401 (2012).
37. W. Liu and D. Zuckerbrod, *J.Electrochem.Soc.*, **152**, 6 (2005).
38. M. Cai, M. S. Ruthkosky, B. Merzougui, S. Swathirajan, M. P. Balogh and S. H. Oh, *J.Power Sources.*, **160**, 2 (2006).
39. C. Chen and T. Fuller, *ECS Transactions.*, **11**, 1 (2007).
40. T. Arlt, M. Klages, I. Manke, M. Messerschmidt, H. Riesemeier, A. Hilger, J. Scholta and J. Banhart, *ECS Transactions.*, **53**, 30 (2013).
41. H. Liu, M. G. George, N. Ge, J. Lee, R. Banerjee, S. Chevalier, P. Shrestha, D. Muirhead, R. Zeis, M. Messerschmidt, J. Scholta and A. Bazylak, **ECS PRIME** (2016 (Submitted)).
42. J. P. Owejan, T. Trabold, D. Jacobson, M. Arif and S. Kandlikar, *Int J Hydrogen Energy.*, **32**, 17 (2007).
43. J. P. Owejan, T. A. Trabold and M. M. Mench, *Int.J.Heat Mass Transfer.*, **71** (2014).
44. P. Antonacci, S. Chevalier, J. Lee, N. Ge, J. Hinebaugh, R. Yip, Y. Tabuchi, T. Kotaka and A. Bazylak, *Electrochim.Acta.*, **188** (2016).
45. X. Yuan, H. Wang, J. Colin Sun and J. Zhang, *Int J Hydrogen Energy.*, **32**, 17 (2007).
46. P. Antonacci, S. Chevalier, J. Lee, R. Yip, N. Ge and A. Bazylak, *Int J Hydrogen Energy.*, **40**, 46 (2015).
47. M. V. Williams, E. Begg, L. Bonville, H. R. Kunz and J. M. Fenton, *J.Electrochem.Soc.*, **151**, 8 (2004).
48. U. Beuscher, *J.Electrochem.Soc.*, **153**, 9 (2006).
49. J. St-Pierre, B. Wetton, G. Kim and K. Promislow, *J.Electrochem.Soc.*, **154**, 2 (2007).
50. D. R. Baker, D. A. Caulk, K. C. Neyerlin and M. W. Murphy, *J.Electrochem.Soc.*, **156**, 9 (2009).
51. S. Chevalier, N. Ge, J. Lee, P. Antonacci, R. Yip, M. George, H. Liu, R. Banerjee, M. Fazeli and A. Bazylak, *Electrochemistry Communications.*, **59** (2015).
52. J. Hinebaugh, J. Lee and A. Bazylak, *J.Electrochem.Soc.*, **159**, 12 (2012).
53. J. Lee, J. Hinebaugh and A. Bazylak, *J.Power Sources.*, **227** (2013).

54. J. Lee, R. Yip, P. Antonacci, N. Ge, T. Kotaka, Y. Tabuchi and A. Bazylak, *J.Electrochem.Soc.*, **162**, 7 (2015).
55. T. Mukaide, S. Mogi, J. Yamamoto, A. Morita, S. Koji, K. Takada, K. Uesugi, K. Kajiwara and T. Noma, *Journal of synchrotron radiation.*, **15**, 4 (2008).
56. C. Hartnig, I. Manke, R. Kuhn, N. Kardjilov, J. Banhart and W. Lehnert, *Appl.Phys.Lett.*, **92**, 13 (2008).
57. J. Hinebaugh, J. Lee, C. Mascarenhas and A. Bazylak, *Electrochim.Acta.*, **184** (2015).
58. H. Markötter, J. Haussmann, R. Alink, C. Tötzke, T. Arlt, M. Klages, H. Riesemeier, J. Scholta, D. Gerteisen and J. Banhart, *Electrochemistry Communications.*, **34** (2013).
59. J. Eller, J. Roth, F. Marone, M. Stampanoni, A. Wokaun and F. N. Büchi, *J.Power Sources.*, **245** (2014).
60. T. W. Wysokinski, D. Chapman, G. Adams, M. Renier, P. Suortti and W. Thomlinson, *Nuclear Instruments and Methods in Physics Research Section A: Accelerators, Spectrometers, Detectors and Associated Equipment.*, **582**, 1 (2007).
61. D. Swinehart, *J.Chem.Educ.*, **39**, 7 (1962).
62. N. Ge, S. Chevalier, J. Hinebaugh, R. Yip, J. Lee, P. Antonacci, T. Kotaka, Y. Tabuchi and A. Bazylak, *Journal of synchrotron radiation.*, **23**, 2 (2016).